EDITOR'S CHOICE

Haem oxygenase limits *Mycobacterium marinum* infection-induced detrimental ferrostatin-sensitive cell death in zebrafish

Kaiming Luo[1,2], Roland Stocker[2,3], Warwick J. Britton[1,4], Kazu Kikuchi[2,5] and Stefan H. Oehlers[1,6] (iD)

1 Tuberculosis Research Program at the Centenary Institute, The University of Sydney, Camperdown, NSW, Australia
2 Victor Chang Cardiac Research Institute, Darlinghurst, NSW, Australia
3 The Heart Research Institute, Newtown, NSW, Australia
4 Department of Clinical Immunology, Royal Prince Alfred Hospital, Camperdown, NSW, Australia
5 National Cerebral and Cardiovascular Center, Suita, Osaka, Japan
6 Infection, Immunity and Inflammation Theme and Sydney Institute for Infectious Diseases, The University of Sydney, Camperdown, NSW, Australia

Iron homeostasis is essential for both sides of the host–pathogen interface. Restricting access of iron slows bacterial growth while iron is also a necessary cofactor for host immunity. Haem oxygenase 1 (HMOX1) is a critical regulator of iron homeostasis that catalyses the liberation of iron during degradation of haem. It is also a stress-responsive protein that can be rapidly upregulated and confers protection to the host. Although a protective role of HMOX1 has been demonstrated in a variety of diseases, the role of HMOX1 in *Mycobacterium tuberculosis* infection is equivocal across experiments with different host–pathogen combinations. Here, we use the natural host–pathogen pairing of the zebrafish-*Mycobacterium marinum* infection platform to study the role of zebrafish haem oxygenase in mycobacterial infection. We identify zebrafish Hmox1a as the relevant functional paralog of mammalian HMOX1 and demonstrate a conserved role for Hmox1a in protecting the host from *M. marinum* infection. Using genetic and chemical tools, we show zebrafish Hmox1a protects the host against *M. marinum* infection by reducing infection-induced iron accumulation and ferrostatin-sensitive cell death.

Introduction

Infection with pathogenic mycobacteria, such as *Mycobacterium tuberculosis* (*Mtb*), leads to the formation of granulomas, the hallmark histological feature of tuberculosis (TB) [1]. Host cells within granulomas undergo significant phenotypic remodelling including the upregulation of cytoprotective stress response proteins in response to mycobacterial virulence factors and changes to the microenvironment [2–4].

Haem oxygenase 1 (HMOX1), a key regulator of iron homeostasis and cellular redox biology, is expressed within human- and mouse-*Mtb* granulomas [3–9]. HMOX1-derived carbon monoxide inhibits the growth of mycobacteria by direct toxicity and inducing mycobacterial dormancy gene expression [10–12]. HMOX1-deficient mice are more susceptible to mycobacterial infection, while inhibition of HMOX1 activity with tin protoporphyrin (SnPP) increases host resistance to mycobacterial infection in human macrophages and mouse models [3–6,8–10,13]. It is unclear whether these contrasting effects on *Mtb* infection are a function of losing nonenzymatic
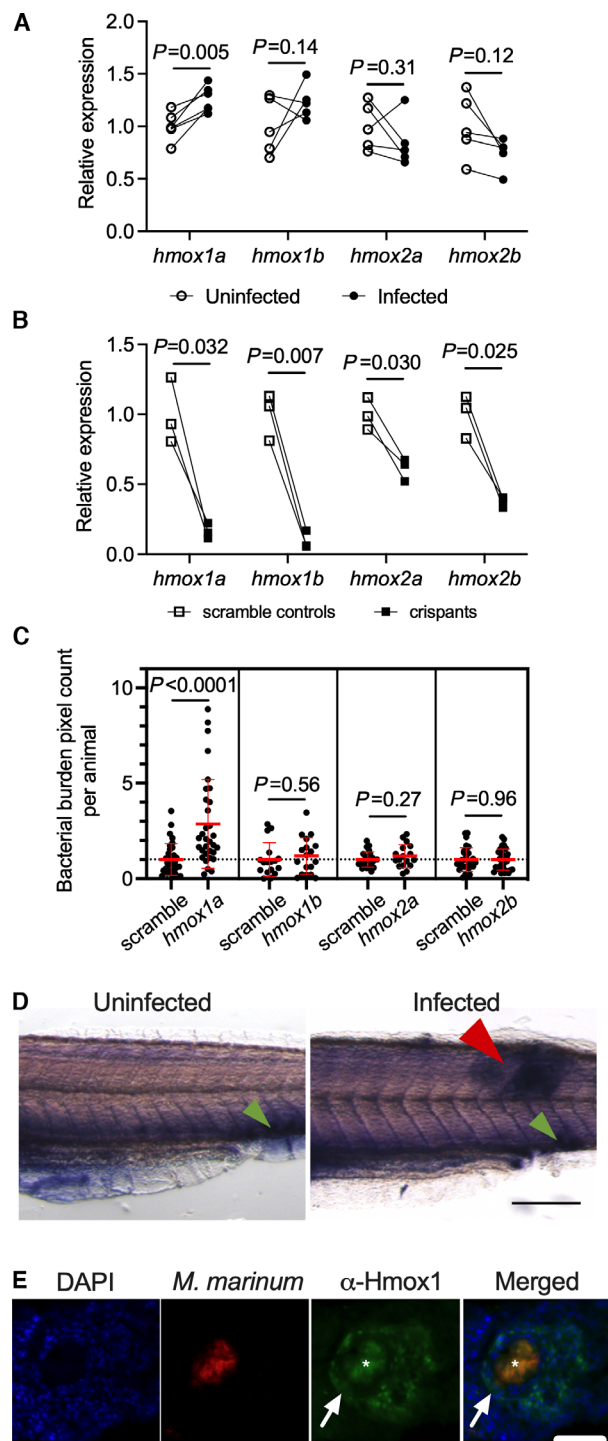
Fig. 1. Zebrafish *hmox1a* is the functional paralog of mammalian *HMOX1* during mycobacterial infection. (A) qPCR expression analysis of zebrafish *hmox* paralogs in homogenates of 14 dpi adult zebrafish infected with *M. marinum*. Biological pairs indicated by matching lines. Matched *t*-test. (B) qPCR expression analysis of zebrafish *hmox* paralogs in 7 dpf crispants. Biological pairs indicated by matching lines. Matched *t*-test. (C) *M. marinum* burden measured by fluorescent pixel count in 5 dpi crispants. Student's *t*-test, data are pooled from two biological replicates per comparison. (D) Whole mount *in situ* hybridisation detection of *hmox1a* transcripts in 5 dpi zebrafish embryos. Green arrowhead indicates site of constitutive CHT expression, and red arrowhead indicates site of inducible expression at a granuloma. Scale bar represents 200 μm. (E) Representative image of antibody detection of Hmox1 in a granuloma of a 14 dpi adult zebrafish. Arrows indicate cellular rim of granuloma. Asterisk indicates bleed through fluorescence of *M. marinum*-TdTomato signal in necrotic core. Scale bar represents 100 μm.

is responsive to a range of oxidative stress-inducing conditions [15–17]. The zebrafish-*M. marinum* model has been widely used to study conserved host redox perturbations associated with mycobacterial infection [18–20]. Here, we have used zebrafish to investigate the role of Hmox1a in the control of mycobacterial infection. We provide evidence that induction of host Hmox1a expression restricts iron supply to limit mycobacterial growth and may prevent excessive ferroptosis.

Results

Zebrafish *hmox1a* is the functional Hmox paralog in *M. marinum* infection

Zebrafish have four Hmox-encoding paralogs: *hmox1a*, *hmox1b*, *hmox2a* and *hmox2b* [15–17]. To determine which paralog is functional in *M. marinum* infection, we first infected adult zebrafish by intraperitoneal injection and analysed gene expression changes at 14 days postinfection (dpi). Infected adults had increased expression of *hmox1a*, but not the other paralogs (Fig. 1A).

To investigate the function of each paralog during *M. marinum* infection, we next used CRISPR/Cas9 technology to knockdown each paralog and infected crispant embryos with *M. marinum* (Fig. 1B). Knockdown of *hmox1a* increased the bacterial burden at 5 dpi, while knockdown of *hmox1b*, *hmox2a* and *hmox2b* did not affect bacterial burden (Fig. 1C).

To investigate *hmox1a* expression in more detail, whole mount *in situ* hybridisation was used to visualise the spatial distribution of *hmox1a* expression within *M. marinum*-infected embryos. *hmox1a* was highly expressed in the haematopoietic niche of the caudal

HMOX1 functions in the gene-deficient mice, differences in infection models or other reasons [14].

HMOX1 is a highly evolutionarily conserved enzyme that has been identified in a wide variety of organisms. Zebrafish *hmox1a* and *hmox1b* encode paralogs of mammalian HMOX1, and their transcription

haematopoietic tissue and around granulomas (Fig. 1D). To spatially examine Hmox expression in adult granulomas, we used a mouse Hmox1 antibody which would potentially detect both Hmox1a and Hmox1b in zebrafish. Hmox1 staining was detected within the host cellular rim of granulomas from 14 dpi zebrafish adults (Fig. 1E).

Hmox1a is required for *M. marinum* granuloma formation in adult zebrafish

To investigate the function of *hmox1a* in the formation of adult zebrafish-*M. marinum* granulomas, we utilised our *hmox1a*^{vcc42} knockout allele [21]. As expected from

our CRISPR-Cas9 knockdown studies, *hmox1a*$^{vcc42/vcc42}$ embryos displayed significantly increased bacterial burden compared with WT clutch mates (Fig. 2A). Adult *hmox1a*$^{vcc42/vcc42}$ mutants had increased mortality following infection that was consistent with the increased bacterial burden (Fig. 2B). Heterozygous *hmox1a*$^{+/vcc42}$ zebrafish displayed intermediate phenotypes in both assays (Fig. 2A,B).

Failure to form granulomas has been proposed to underlie the mycobacterial control defect in *Hmox1*-null mice [3,4]. To determine whether zebrafish reproduced this phenotype, we scored *M. marinum* granulomas as 'organised' or 'loose' based on host nuclear structure in *hmox1a*$^{vcc42/vcc42}$ and their WT clutch
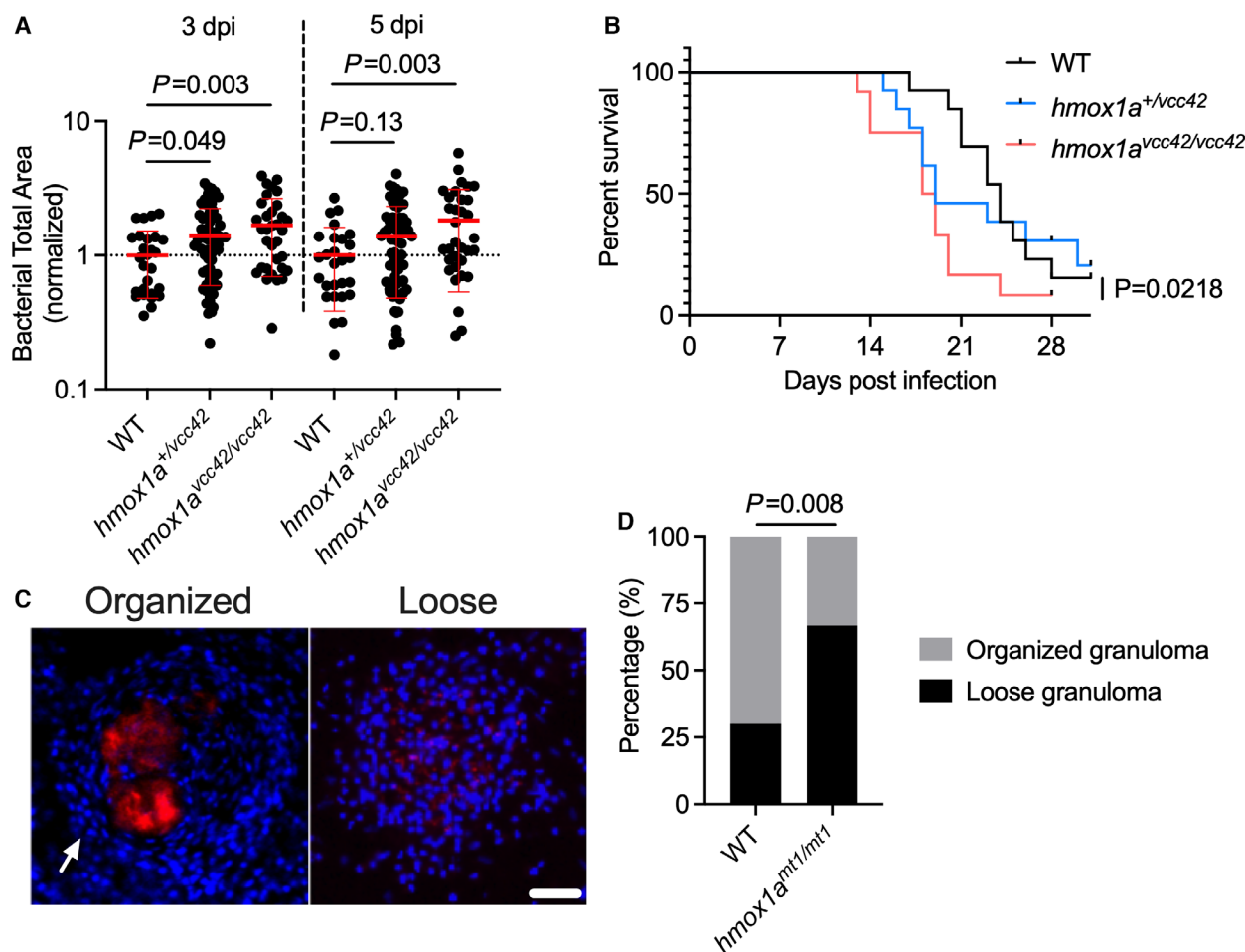

Fig. 2. Zebrafish Hmox1a is necessary for efficient granuloma formation. (A) Bacterial burden in 5 dpi *hmox1a*$^{vcc41/vcc42}$ mutant embryos. ANOVA test performed for each timepoint, data are pooled from 3 experiments. (B) Survival of adult *hmox1a*$^{vcc41/vcc42}$ mutant zebrafish following infection with *M. marinum*. *n* = 13 WT, 13 heterozygous mutants, 12 homozygous mutants. Log-rank test, single replicate. (C) Representative images of granuloma morphology classes in 14 dpi *hmox1a*$^{vcc41/vcc42}$ mutant adult zebrafish. Arrow indicates organised cellular rim of granuloma. Scale bar represents 50 μm. (D) Quantification of granuloma morphology classes in 14 dpi *hmox1a*$^{vcc41/vcc42}$ mutant adult zebrafish. Comparison by Fisher's test on total granuloma counts, *n* = 40 WT granulomas from 3 animals, 24 *hmox1a*$^{vcc41/vcc42}$ mutant granulomas from 3 animals.

mates (Fig. 2C) [2,22]. The proportion of unorganised 'loose' granulomas in *hmox1a*[vcc42/vcc42] adults was significantly higher than in the WT adults demonstrating a conserved defect in granuloma formation (Fig. 2D).

Hmox1a-dependent *M. marinum* granuloma formation does not explain increased susceptibility to infection

Regev *et al.* have proposed abnormal macrophage migration to mycobacteria as an underlying defect prior to in the hypersusceptibility of HMOX1-deficient mice [3]. We took advantage of the visual accessibility of zebrafish embryos to quantify macrophage containment of infection in *Tg(mpeg1.1:egfp)*[vvc7] embryos where macrophages are labelled by GFP expression. The proportion of *M. marinum* that colocalised with GFP-positive macrophages was similar between WT and *hmox1a*[vcc42/vcc42] homozygous larvae at 5 dpi, demonstrating Hmox1a

does not grossly alter the recruitment of macrophages to *M. marinum* infection (Fig. 3A).

To further investigate the association between *hmox1a* and granuloma formation, we infected *hmox1a*[vcc42/vcc42] embryos with ΔESX1 *M. marinum*, a strain that is unable to drive granuloma formation [23]. Unexpectedly, ΔESX1 *M. marinum* load was significantly increased in *hmox1a*[vcc42/vcc42] homozygous larvae at both 3 and 5 dpi suggesting a more general susceptibility to mycobacterial infection than a defect in granuloma formation alone (Fig. 3B). Again, there was no defect in macrophage containment of ΔESX1 *M. marinum* foci (Fig. 3C).

To further explore whether *hmox1a* deficiency affected susceptibility to other bacterial pathogens that do not form granulomas in zebrafish, we infected embryos with uropathogenic *Escherichia coli* (UPEC) strain UTI-89 which causes an acute lethal infection of zebrafish embryos [24]. We observed decreased survival
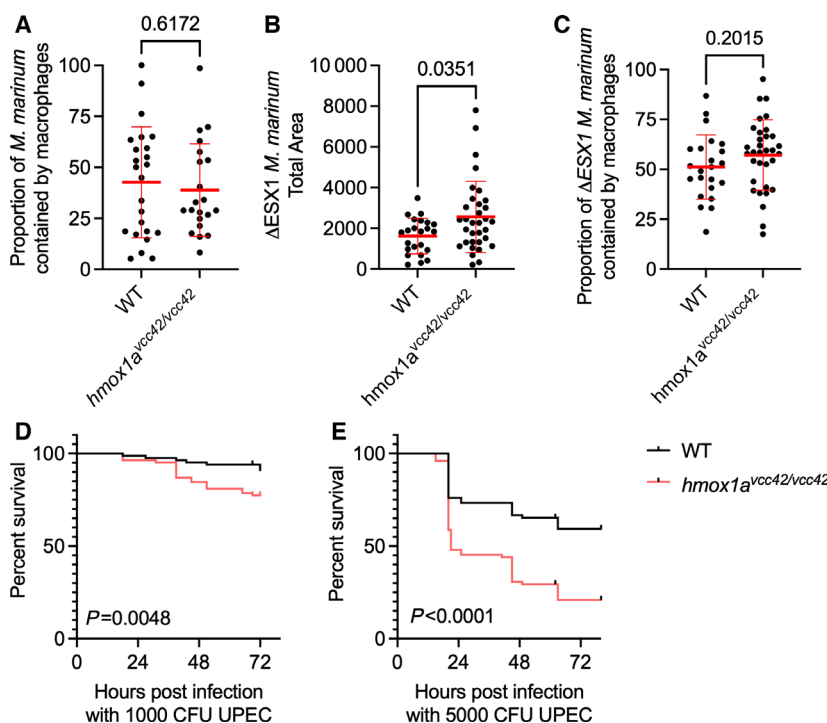

Fig. 3. Increased infection susceptibility in *hmox1a* mutants is not dependent on granuloma formation. (A) Quantification of *M. marinum* containment by *mpeg1.1:gfp*-positive macrophages in 5 dpi *hmox1a*[vcc41/vcc42] mutant embryos. Student's *t*-test, data are pooled from two biological replicates. (B) Bacterial burden in *hmox1a* crispants infected with ΔESX1 *M. marinum*. Student's *t*-test, data are representative of three biological replicates. (C) Quantification of ΔESX1 *M. marinum* containment by *mpeg1.1:gfp*-positive macrophages in 5 dpi *hmox1a*[vcc41/vcc42] mutant embryos. Student's *t*-test, data are pooled from two biological replicates. (D) Survival curve of 2 dpf *hmox1a*[vcc41/vcc42] mutant embryos infected with 1000 CFU UPEC. Log-rank test, *n* = 84 embryos each group, data are pooled from two biological replicates. (E) Survival curve of 2 dpf *hmox1a*[vcc41/vcc42] mutant embryos infected with 5000 CFU UPEC. Log-rank test, *n* = 75 embryos each group, data are pooled from two biological replicates.

of *hmox1a^vcc42/vcc42* embryos compared with WT embryos across two doses of UPEC (Fig. 3D,E).

Hmox1a restricts iron to control *M. marinum* infection

Since HMOX1 is a key regulator of iron homeostasis, we performed Perls' Prussian Blue staining on sections from WT and *hmox1a^vcc42/vcc42* adults to visualise free iron (Fig. 4A). There were more Perls' Prussian Blue-positive granulomas in *hmox1a^vcc42/vcc42* mutants than WT zebrafish (Fig. 4B). Perls' Prussian Blue staining of *M. marinum*-infected embryos was not as vivid as that of adult granulomas (Fig. 4C), but spectral quantification staining detected more Perls' Prussian Blue staining in granulomas from *hmox1a* crispants (Fig. 4D).

To confirm the presence of increased iron at the host–pathogen interface, we performed gene expression analysis of *aco1*, a host iron-suppressed regulator of iron metabolism [25], which was downregulated in 5 dpi *hmox1a^vcc42/vcc42* embryos (Fig. 4E). To investigate the bacterial response, we profiled the expression of *bfrB*, an iron storage gene in *M. marinum* homologous to human ferritin. The expression of *bfrB* was progressively increased from 1 to 3 to 5 dpi and was higher in *hmox1a* crispants than WT hosts at 5 dpi (Fig. 4F).

Mycobacteria require iron as a redox cofactor for vital enzymes and utilise multiple strategies to acquire iron from haem which may compete with host Hmox1a-mediated degradation of haem [26,27]. We first tested the susceptibility of Hmox1a-deficient embryos when challenged with an exogenous source of bioavailable iron by the addition of hemin. Hemin supplementation increased *M. marinum* burden in *hmox1a* crispants but not scrambled controls demonstrating a genotype-specific susceptibility to the addition of exogenous hemin (Fig. 4G).
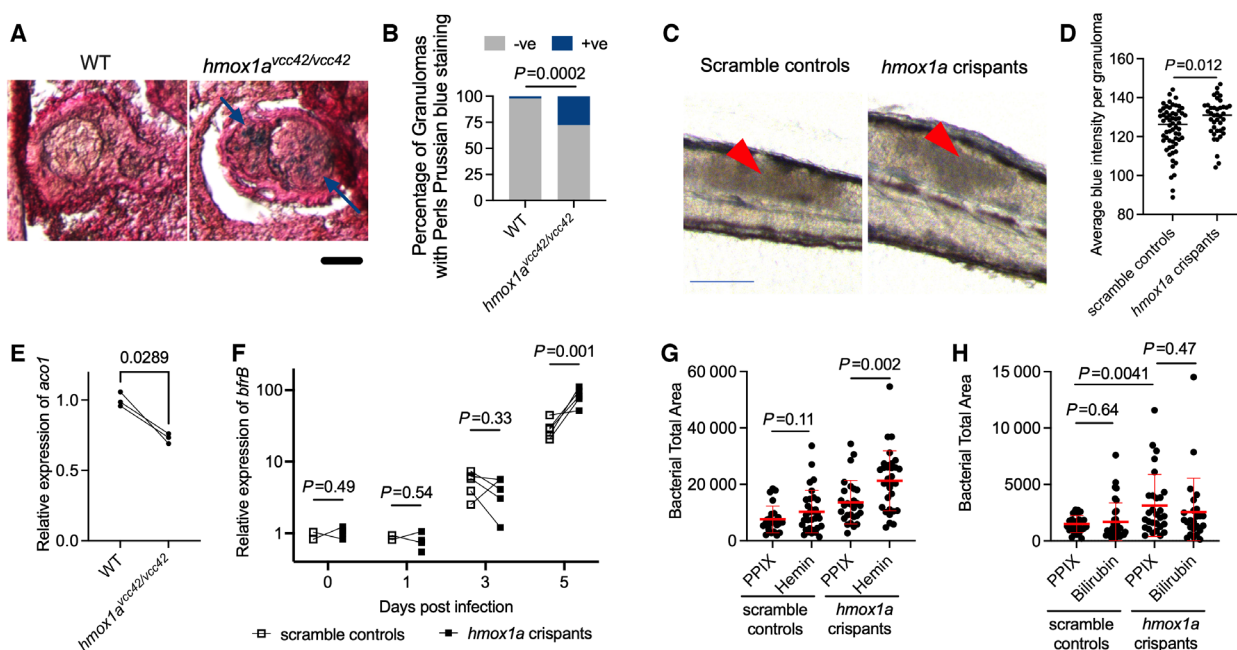

Fig. 4. Zebrafish Hmox1a restricts iron availability during *M. marinum* infection. (A) Representative images of Perls' Prussian Blue staining of granulomas from 14 dpi *hmox1a^vcc41/vcc42* mutant adult zebrafish. Blue arrows indicate location of positive staining. Scale bar represents 50 μm. (B) Quantification of granuloma Perls' Prussian Blue staining in *hmox1a^vcc41/vcc42* mutant adult zebrafish. Comparison by Fisher's test on total granuloma counts, *n* = 46 granulomas from 3 WT animals, 83 granulomas from 3 *hmox1a^vcc41/vcc42* mutants. (C) Representative images of Perls' Prussian Blue staining of 5 dpi zebrafish embryos. Red arrows indicate locations of analysed granulomas. Scale bar represents 100 μm. (D) Quantification of granuloma Perls' Prussian Blue staining in 5 dpi *hmox1a* crispants. Each data point represents a single granuloma from an individual embryo. Student's *t*-test, data are pooled from three biological replicates. (E) qPCR analysis of host *aco1* gene expression in 5 dpi *hmox1a^vcc41/vcc42* mutant embryos. Matched *t*-test. (F) qPCR analysis of *M. marinum bfrB* gene expression in *hmox1a* crispants. Matched *t*-test at each timepoint. (G) Bacterial burden in 5 dpi *hmox1a* crispants treated with 10 μM hemin. Comparison by ANOVA, each point represents a single zebrafish, data are representative of three biological replicates with crispants and two biological replicates with *hmox1a^vcc41/vcc42* mutant embryos. (H) Bacterial burden in 5 dpi *hmox1a* crispants treated with 10 μM bilirubin. Comparison by ANOVA, each point represents a single zebrafish, data are representative of three biological replicates with crispants and two biological replicates with *hmox1a^vcc41/vcc42* mutant embryos.

In addition to producing free iron which is sequestered by ferritin [28], HMOX1 catalyses the production of the important antioxidants carbon monoxide and biliverdin from hemin. We next examined the effect of supplementing bilirubin, the breakdown product of HMOX1-produced biliverdin, into our zebrafish-*M. marinum* infection system. We did not observe any effects of bilirubin treatment on *M. marinum* burden in control and *hmox1a*-depleted larvae (Fig. 4H).

Hmox1a deficiency exposes hosts to *M. marinum* infection-induced ferrostatin-sensitive cell death

Excessive iron can be toxic to host cells by triggering ferroptosis, a recently described mode of cell death associated with lipid peroxidation that drives pathology in the mouse-*Mtb* model [29,30]. We hypothesised ferroptosis could be responsible for the increased *M. marinum* burden in our Hmox1a-deficient zebrafish.

Consistent with the increased iron in Hmox1a-deficient zebrafish, we observed increased granuloma CellROX staining in *hmox1a* crispants compared with control embryos (Fig. 5A). We also observed more TUNEL-positive cells around granulomas in *hmox1a* crispants (Fig. 5B).

To test the role of ferroptosis in these phenotypes, we treated embryos with ferrostatin, a small molecule inhibitor of ferroptosis. Ferrostatin treatment reduced bacterial burden in *hmox1a* crispants but not in scramble controls (Fig. 5C). Ferrostatin treatment also reduced CellROX staining in granulomas and the
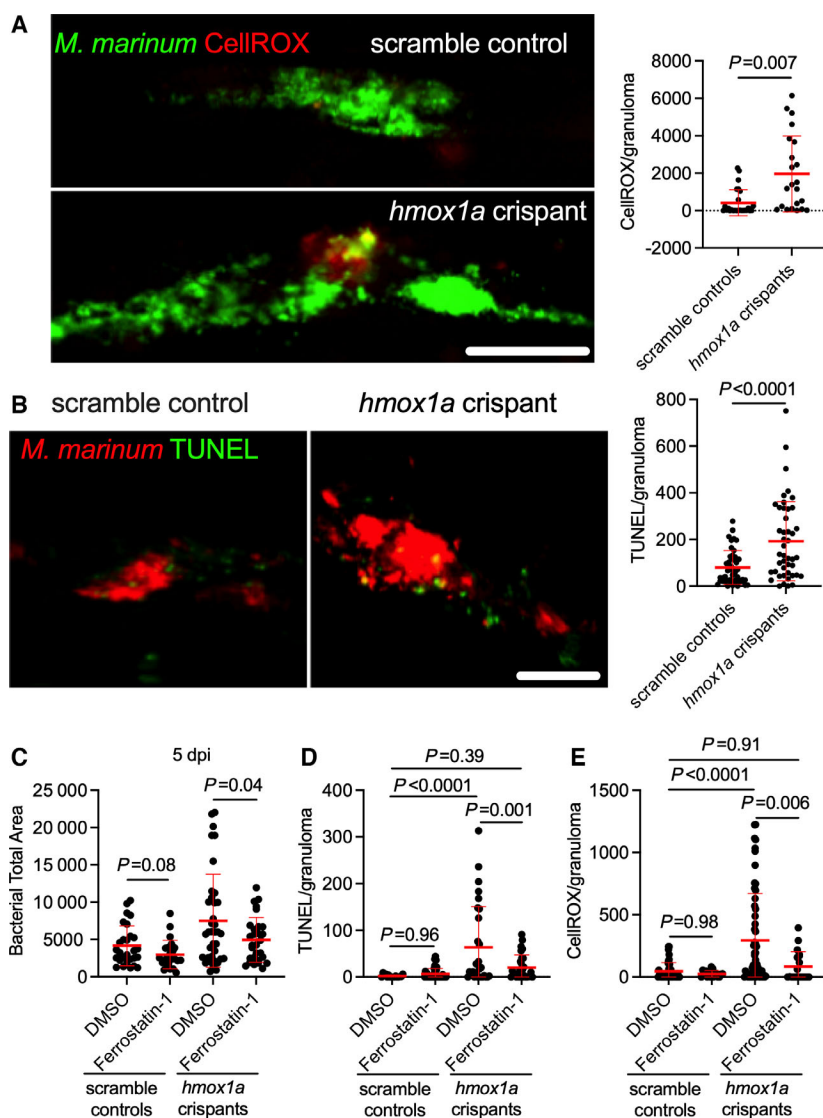

Fig. 5. Zebrafish Hmox1a prevents *M. marinum* infection-induced ferrostatin-sensitive cell death. (A) Representative images and quantification of CellROX staining in 5 dpi *hmox1a* crispants. Scale bar represents 50 μm. Comparison by Student's *t*-test, each point represents a single granuloma from a single zebrafish. (B) Representative images and quantification of TUNEL staining in 5 dpi *hmox1a* crispants. Scale bar represents 50 μm. Comparison by Student's *t*-test, each point represents a single granuloma from a single zebrafish, data are pooled from two biological replicates. (C) Bacterial burden in 5 dpi *hmox1a* crispants treated with ferrostatin-1. Comparison by ANOVA, each point represents a single zebrafish, data are representative of two biological replicates. (D) Quantification of CellROX staining in 5 dpi *hmox1a* crispants treated with ferrostatin-1. Comparison by ANOVA, each point represents a single granuloma from a single zebrafish, data are representative of two biological replicates. (E) Quantification of TUNEL staining in 5 dpi *hmox1a* crispants treated with ferrostatin-1. Comparison by ANOVA, each point represents a single granuloma from a single zebrafish, data are representative of two biological replicates.

number of TUNEL-positive cells per granuloma (Fig. 5D,E).

Discussion

Host cells need to balance iron availability and the production of reactive oxygen species during infection with intracellular pathogens. Our data show infection-induced Hmox1a is a host-protective enzyme that aids containment of infection within granulomas and slows the growth of *M. marinum* by restricting iron availability and preventing ferrostatin-sensitive cell death.

Our study clearly identifies zebrafish *hmox1a* as the functional ortholog of mammalian HMOX1 as the most transcriptionally responsive to infection in adult zebrafish and the only gene which had a knockdown burden phenotype in the CRIPSR-Cas9 embryo infection model. Our data further suggest zebrafish *hmox1b* does not functionally compensate for loss of *hmox1a* and may be a pseudogene.

Our experiment infecting *hmox1a*-deficient zebrafish with the ΔESX1 *M. marinum* suggests *hmox1a* is involved in control of *M. marinum* infection upstream of granuloma formation. We found iron accumulation in *M. marinum* granulomas which correlated with Cell-ROX staining and increased cell death in *hmox1a*-deficient zebrafish. These phenotypes were reversed after treatment with ferrostatin, suggesting the *M. marinum* control defect in *hmox1a*-deficient zebrafish could be driven by iron-induced ferroptosis upstream of granuloma formation.

While our finding that supplementation with biliverdin, a product of HMOX1-mediated catabolism of haem, did not affect *M. marinum* burden in *hmox1a*-deficient embryos, additional work is warranted to investigate the role of HMOX1-mediated carbon monoxide production in the zebrafish-*M. marinum* model. Carbon monoxide has direct inhibitory effects on the growth of *M. tuberculosis* in mouse infection models [10–12], and it would be fascinating to study this interaction in the natural host–pathogen pairing of the zebrafish-*M. marinum* infection model.

Our infection studies with UPEC suggest a more generalised immunodeficiency in *hmox1a*-deficient zebrafish. Further work is required to determine the exact mechanisms of susceptibility to individual pathogens and the potential for ferroptotic involvement in the pathogenesis of specific pathogens.

The nonspecific action of ferrostatin-1 is a potential limitation of our study. Ferrostatin-1 has been recently reported to inhibit the enzymic activity of 15-lipoxygenase, which produces the HpETE-PE ferroptotic cell death signal as part of the 15LOX/PEBP1

complex with iron as a cofactor [31,32]. Infection-induced lipoxygenase and cyclooxygenase activity in mycobacterial infection generally leads to unfavourable suppression of inflammation, while inhibition of these enzyme families generally controls mycobacterial infection [33–37]. Thus, we are unable to rule out 15LOX/PEBP1-induced ferroptosis as a possible mechanism of ferrostatin-induced protection in our *hmox1a*-deficient zebrafish. Additionally, we did not detect lipid peroxidation in zebrafish embryos which would be expected during ferroptosis.

The lack of host protection in WT embryos treated with ferrostatin suggests ferroptosis, or at least ferrostatin-inhibitable cell death, may be of limited importance in the zebrafish embryo-*M. marinum* infection model. Our data suggest depletion of Hmox1a is required to sensitise embryos to biologically significant levels of iron stress-induced cell death by impairing endogenous iron metabolism. Similarly, the *hmox1a*-deficient genotype-specific response to hemin supplementation suggests the presence of sufficient iron buffering ability in WT zebrafish embryos during *M. marinum* infection. This sufficient iron buffering ability may explain why any increase in free iron production by WT Hmox1a in our hemin supplementation experiments did not significantly increase the burden of *M. marinum*.

The results from the infection time course highlight 3–5 dpi as a key window in *M. marinum* infection when granulomas undergo extensive organisation and expansion. During this time period, host *hmox1a* and bacterial *bfrB* are highly upregulated, and *hmox1a*-deficient zebrafish embryos develop their conditional pathologies. Together, these data provide evidence of haem oxygenase function in the race to acquire iron between host and mycobacterium during granuloma formation.

Materials and methods

Zebrafish husbandry

Adult zebrafish were maintained at Centenary Institute, and embryos were obtained by natural spawning followed and raised in E3 media at 28–32 °C (Sydney Local Health District AWC Approvals: 16-037 and 17-036). Zebrafish lines used were as follows: *Tg(mpeg1.1:egfp)*[vcc7] [38], *hmox1a*[vcc42] [21].

Bacterial infection

Single cell suspensions of mid log-phase fluorescent *M. marinum* strains and ΔESX1 *M. marinum* were prepared

and stored at −80 °C in aliquots as previously described [39]. Zebrafish infections were carried out as previously described with 200 CFU infection doses by microinjection into the caudal vein of zebrafish embryos or intraperitoneal injection into adults for *M. marinum* [22,39]. Infected adults were maintained at 28 °C with 14 : 10-h light : dark lighting cycle.

UPEC strain UTI-89 carrying the pGI6/mCherry spectinomycin resistance plasmid [24] was cultured overnight in LB media supplemented with 50 µg·mL^{-1} spectinomycin at 37 °C with 200 RPM shaking. Overnight cultures were diluted 1 : 100 into fresh LB media supplemented with 50 µg·mL^{-1} spectinomycin and outgrown for 3 h at 37 °C with 200 RPM shaking, harvested by centrifugation, rinsed in PBS and microinjected into the caudal vein of zebrafish embryos at the concentrations indicated.

Quantitative Real-time PCR

Total RNA was extracted from homogenates using TRIzol (Thermo Fisher Scientific, Waltham, MA), and cDNA was synthesised with a High Capacity cDNA Synthesis Kit (Thermo Fisher Scientific). qPCRs were performed on a LightCycler® 480 System. Gene expression was quantified by the delta–delta C_T method using normalisation to zebrafish *bact* or *M. marinum 18s* as appropriate. Sequences of primers are listed in Table 1.

Histology

Cryosectioning was performed as previously described [22]. Hmox1 immunostaining was carried out with a mouse anti-HMOX1 primary (GeneTex GTX633693) and a goat anti-mouse Alexa Fluor 488 (Thermo Fisher Scientific, R37120). Perls' Prussian Blue staining was performed in acid ferrocyanide solution (equal amount of 5% aqueous potassium ferrocyanide and 5% HCl) for 30 min at room temperature followed by two washes of distilled water and counterstaining with 0.1% nuclear fast red. Whole mount embryo Perls' Prussian Blue staining was performed without the counterstaining step.

CRISPR/Cas9 Gene Knockdown

The gRNA target sites for each gene were designed using CRISPRscan. The sequences of gRNA oligonucleotides are listed in Table 2. The gRNA templates were amplified by PCR with scaffold reverse primer and then transcribed with HiScribe™ T7 High Yield RNA Synthesis Kit (NEB) [40]. One cell stage embryos were injected with 1 nL of a mixture containing 200 ng·µL^{-1} of the four gRNAs and 2 ng·µL^{-1} Cas9 (Sigma, IDT or Sydney Analytical).

Imaging

Imaging was carried out on Leica M205FA and DM6000B, and DeltaVision Elite microscopes as previously described [18,22,39].

Image analysis

Fluorescent pixel count for enumeration of bacterial burden and quantification of fluorescent staining was carried out as previously described in IMAGEJ [39]. Fluorescent stain areas are reported as pixels per granuloma.

Macrophage containment of *M. marinum* was calculated as the proportion of bacterial fluorescence that overlapped with *mpeg1.1:egfp* fluorescence signal. ImageJ was used to threshold GFP images followed by the 'Clear Outside' then 'Create Selection' and 'Add to roiManager' commands to define the bounds of macrophage cells. We then quantified the bacterial fluorescence within these bounds by fluorescent pixel count.

Perls' Prussian Blue staining in embryos was quantified by splitting the blue channel from colour images and then using the 'Measure' function in IMAGEJ to quantify the inverse mean pixel intensity of a constant area within granulomas. The 'average blue intensity per granuloma' was calculated by subtracting the background blue pixel intensity from the granuloma blue pixel intensity.

Whole mount in situ hybridisation

Sequences of primers used to generate the DIG-labelled *hmox1a* probe are listed in Table 1; *in situ* hybridisation was carried out as previously described [41].

Table 1. Primers used for gene expression studies.

Gene	Forward primer 5′–3′	Reverse Primer 5′–3′
hmox1a F2/R2	GGGCAGGACTTGGAGCACTT	GGACTGCTCTTGCCAATCTCT
hmox1a F3/R2	TAAAAACGAAGTGGGGCGGT	TGTTCAGACAGATCACTGCCA
hmox1b	AGCTACCAGAGGGGCCGAGT	CGCCTCGTAGATCTTGTAGAGC
hmox2a	ATGGCGGTCAGTGGAAACACAACC	GGCAACAGCAGCAACCAATGTGGC
hmox2b	TTTAGGAGGTTGAGTTGGAGTCAG	TTCTGCCTTCTGGTGCACTTCT
aco1	CTGGTGAAGCAGGACGATGT	GGTACACCCGTGAAGTCCTG
bfrB (*M. marinum*)	TTGGCGAAGCACTTTTACGC	GGAATCTCGACACGGAGGTC
18s	TCGCTAGTTGGCATCGTTTATG	CGGAGGTTCGAAGACGATCA
hmox1a for ISH probe	TCCCCGCGGGTGAAACTGGCTCAACATTTTCACT	CCATCGATACATACAGAAGACAACTCAAAGCGT

Table 2. Primer sequences used for CRISPR-Cas9 knockdown. Blue and green sequences indicate common backbone sequence.

Primer name	Sequence 5′–3′
hmox1a target 1	TAATACGACTCACTATAGGACTCCACCAAAAGCAAAGGTTTTAGAGCTAGAA
hmox1a target 2	TAATACGACTCACTATAGGGTGTTTTCAGCTCTGACGGTTTTAGAGCTAGAA
hmox1a target 3	TAATACGACTCACTATAGGAGATCTACCGAGCGCTGGGTTTTAGAGCTAGAA
hmox1a target 4	TAATACGACTCACTATAGGTAAATGGGCTGCACTGCTGTTTTAGAGCTAGAA
hmox1b target 1	TAATACGACTCACTATAGGGTCACTGTCGGTGATCTGGTTTTAGAGCTAGAA
hmox1b target 2	TAATACGACTCACTATAGGAGCGTCACTCGGCCCCTCGTTTTAGAGCTAGAA
hmox1b target 3	TAATACGACTCACTATAGGTCTACGAGGCGCTGGAGGGTTTTAGAGCTAGAA
hmox1b target 4	TAATACGACTCACTATAGGTGGGAGCCACGGCATCATGTTTTAGAGCTAGAA
hmox2a target 1	TAATACGACTCACTATAGGAGAAGTTCAAGCCCTCACGTTTTAGAGCTAGAA
hmox2a target 2	TAATACGACTCACTATAGGTTACATGGGTGACCTATCGTTTTAGAGCTAGAA
hmox2a target 3	TAATACGACTCACTATAGGAGGTGGGTCGCGATGACCGTTTTAGAGCTAGAA
hmox2a target 4	TAATACGACTCACTATAGGCATTGGTCCCCATGCACAGTTTTAGAGCTAGAA
hmox2b target 1	TAATACGACTCACTATAGGCAGATCTGTCGGCCTGTAGTTTTAGAGCTAGAA
hmox2b target 2	TAATACGACTCACTATAGGTCGGGGGGGCAGGTGCTCGTTTTAGAGCTAGAA
hmox2b target 3	TAATACGACTCACTATAGGGCAGCGCATTCATCAGATGTTTTAGAGCTAGAA
hmox2b target 4	TAATACGACTCACTATAGGGACGGAAGATGCTGCCAAGTTTTAGAGCTAGAA
scramble target 1	TAATACGACTCACTATAGGCAGGCAAAGAATCCCTGCCGTTTTAGAGCTAGAAATAGC
scramble target 2	TAATACGACTCACTATAGGTACAGTGGACCTCGGTGTCGTTTTAGAGCTAGAAATAGC
scramble target 3	TAATACGACTCACTATAGGCTTCATACAATAGACGATGGTTTTAGAGCTAGAAATAGC
scramble target 4	TAATACGACTCACTATAGGTCGTTTTGCAGTAGGATCGGTTTTAGAGCTAGAAATAGC
Scaffold	AAA AGC ACC GAC TCG GTG CCA CTT TTT CAA GTT GAT AAC GGA CTA GCC TTA TTT TAA CTT GCT ATT TCT AGC TCT AAA AC

Small molecule treatments

Small molecules were added directly to embryo media at final concentrations of: 15 μM protoporphyrin IX (Sigma-Aldrich, St. Louis, MO, USA) and hemin (Fluka, St. Louis, MO, USA), 10 μM bilirubin (Frontier Scientific, Logan, UT, USA) and 1 μM ferrostatin (Sigma-Aldrich). Small molecules were added immediately after infection and refreshed at 3 dpi.

Cell death and reactive oxygen species staining

TUNEL and CellROX (both Thermo Fisher Scientific) staining was performed as previously described and according to manufacturer's instructions [18].

Statistical analysis

Statistical tests were carried out as indicated in figure legends using Prism (GRAPHPAD Software, San Diego, CA). Each data point indicates a single animal unless otherwise stated. Data are plotted as means +/− standard deviation.

Conflict of interest

The authors declare no conflict of interest.

Author contributions

KL performed experiments, analysed data and drafted manuscript. RS supervised project and provided resources. WJB supervised project and provided resources. KK supervised project and provided resources. SHO performed experiments, analysed data, drafted manuscript, supervised project and provided resources. All authors edited the manuscript.

Peer Review

References

1 Ramakrishnan L (2020) Mycobacterium tuberculosis pathogenicity viewed through the lens of molecular Koch's postulates. *Curr Opin Microbiol* **54**, 103–110.

2 Cronan MR, Beerman RW, Rosenberg AF, Saelens JW, Johnson MG, Oehlers SH, Sisk DM, Jurcic Smith KL, Medvitz NA, Miller SE *et al.* (2016) Macrophage Epithelial reprogramming underlies mycobacterial granuloma formation and promotes infection. *Immunity* **45**, 861–876.

3 Regev D, Surolia R, Karki S, Zolak J, Montes-Worboys A, Oliva O, Guroji P, Saini V, Steyn AJ, Agarwal A *et al.* (2012) Heme oxygenase-1 promotes granuloma development and protects against dissemination of mycobacteria. *Lab Invest* **92**, 1541–1552.

4 Silva-Gomes S, Appelberg R, Larsen R, Soares MP & Gomes MS (2013) Heme catabolism by heme oxygenase-1 confers host resistance to Mycobacterium infection. *Infect Immun* **81**, 2536–2545.

5 Costa DL, Namasivayam S, Amaral EP, Arora K, Chao A, Mittereder LR, Maiga M, Boshoff HI, Barry CE 3rd, Goulding CW *et al.* (2016) Pharmacological inhibition of host heme oxygenase-1 suppresses mycobacterium tuberculosis infection in vivo by a mechanism dependent on T lymphocytes, *Mbio* **7**, 41.

6 Abdalla MY, Ahmad IM, Switzer B & Britigan BE (2015) Induction of heme oxygenase-1 contributes to survival of Mycobacterium abscessus in human macrophages-like THP-1 cells. *Redox Biol* **4**, 328–339.

7 Rockwood N, Costa DL, Amaral EP, Du Bruyn E, Kubler A, Gil-Santana L, Fukutani KF, Scanga CA, Flynn JL, Jackson SH *et al.* (2017) Mycobacterium tuberculosis induction of heme oxygenase-1 expression is dependent on oxidative stress and reflects treatment outcomes. *Front Immunol* **8**, 542.

8 Chinta KC, Rahman MA, Saini V, Glasgow JN, Reddy VP, Lever JM, Nhamoyebonde S, Leslie A, Wells RM, Traylor A *et al.* (2018) Microanatomic distribution of myeloid heme oxygenase-1 protects against free radical-mediated immunopathology in human tuberculosis. *Cell Rep* **25**, 1938–1952.

9 Scharn CR, Collins AC, Nair VR, Stamm CE, Marciano DK, Graviss EA & Shiloh MU (2016) Heme Oxygenase-1 regulates inflammation and mycobacterial survival in human macrophages during mycobacterium tuberculosis infection. *J Immunol* **196**, 4641–4649.

10 Shiloh MU, Manzanillo P & Cox JS (2008) Mycobacterium tuberculosis senses host-derived carbon monoxide during macrophage infection. *Cell Host Microbe* **3**, 323–330.

11 Kumar A, Deshane JS, Crossman DK, Bolisetty S, Yan BS, Kramnik I, Agarwal A & Steyn AJ (2008) Heme oxygenase-1-derived carbon monoxide induces the Mycobacterium tuberculosis dormancy regulon. *J Biol Chem* **283**, 18032–18039.

12 Zacharia VM, Manzanillo PS, Nair VR, Marciano DK, Kinch LN, Grishin NV, Cox JS & Shiloh MU (2013) cor, a novel carbon monoxide resistance gene, is essential for Mycobacterium tuberculosis pathogenesis. *Mbio* **4**, e00721–e813.

13 Costa DL, Amaral EP, Namasivayam S, Mittereder LR, Fisher L, Bonfim CC, Sardinha-Silva A, Thompson RW, Hieny SE, Andrade BB *et al.* (2021) Heme oxygenase-1 inhibition promotes IFNgamma- and NOS2-mediated control of Mycobacterium tuberculosis infection. *Mucosal Immunol* **14**, 253–266.

14 Costa DL, Amaral EP, Andrade BB & Sher A (2020) Modulation of inflammation and immune responses by heme oxygenase-1: implications for infection with intracellular pathogens. *Antioxidants (Basel)* **9**, 1205.

15 Mills MG & Gallagher EP (2017) A targeted gene expression platform allows for rapid analysis of chemical-induced antioxidant mRNA expression in zebrafish larvae. *PLoS One* **12**, e0171025.

16 Holowiecki A, O'Shields B & Jenny MJ (2017) Spatiotemporal expression and transcriptional regulation of heme oxygenase and biliverdin reductase genes in zebrafish (Danio rerio) suggest novel roles during early developmental periods of heightened oxidative stress. *Comp Biochem Physiol C Toxicol Pharmacol* **191**, 138–151.

17 Holowiecki A, O'Shields B & Jenny MJ (2016) Characterization of heme oxygenase and biliverdin reductase gene expression in zebrafish (Danio rerio): Basal expression and response to pro-oxidant exposures. *Toxicol Appl Pharmacol* **311**, 74–87.

18 Black HD, Xu W, Hortle E, Robertson SI, Britton WJ, Kaur A, New EJ, Witting PK, Chami B & Oehlers SH (2019) The cyclic nitroxide antioxidant 4-methoxy-TEMPO decreases mycobacterial burden in vivo through host and bacterial targets. *Free Radic Biol Med* **135**, 157–166.

19 Roca FJ & Ramakrishnan L (2013) TNF dually mediates resistance and susceptibility to mycobacteria via mitochondrial reactive oxygen species. *Cell* **153**, 521–534.

20 Roca FJ, Whitworth LJ, Redmond S, Jones AA & Ramakrishnan L (2019) TNF induces pathogenic programmed macrophage necrosis in tuberculosis

through a mitochondrial-lysosomal-endoplasmic reticulum circuit. *Cell* **178**, 1344–1361.

21 Luo K, Ogawa M, Ayer A, Britton WJ, Stocker R, Kikuchi K & Oehlers SH. (2021) Zebrafish heme oxygenase 1a is necessary for normal development and macrophage migration. *bioRxiv* **7**, 802.

22 Cheng T, Kam JY, Johansen MD & Oehlers SH (2020) High content analysis of granuloma histology and neutrophilic inflammation in adult zebrafish infected with Mycobacterium marinum. *Micron* **129**, 102782.

23 Volkman HE, Clay H, Beery D, Chang JC, Sherman DR & Ramakrishnan L (2004) Tuberculous granuloma formation is enhanced by a mycobacterium virulence determinant. *PLoS Biol* **2**, e367.

24 Wright K, de Silva K, Plain KM, Purdie AC, Blair TA, Duggin IG, Britton WJ & Oehlers SH. (2021) Mycobacterial infection-induced miR-206 inhibits protective neutrophil recruitment via the CXCL12/CXCR4 signalling axis. *PLoS Pathog* **12**, 422665.

25 Pantopoulos K (2004) Iron metabolism and the IRE/IRP regulatory system: an update. *Ann N Y Acad Sci* **1012**, 1–13.

26 Marcela Rodriguez G & Neyrolles O (2014) Metallobiology of tuberculosis. *Microbiol Spectr* **2**, 128.

27 Pandey R & Rodriguez GM (2012) A ferritin mutant of Mycobacterium tuberculosis is highly susceptible to killing by antibiotics and is unable to establish a chronic infection in mice. *Infect Immun* **80**, 3650–3659.

28 Seiwert N, Wecklein S, Demuth P, Hasselwander S, Kemper TA, Schwerdtle T, Brunner T & Fahrer J (2020) Heme oxygenase 1 protects human colonocytes against ROS formation, oxidative DNA damage and cytotoxicity induced by heme iron, but not inorganic iron. *Cell Death Dis* **11**, 787.

29 Amaral EP, Costa DL, Namasivayam S, Riteau N, Kamenyeva O, Mittereder L, Mayer-Barber KD, Andrade BB & Sher A (2019) A major role for ferroptosis in Mycobacterium tuberculosis-induced cell death and tissue necrosis. *J Exp Med* **216**, 556–570.

30 Dixon SJ, Lemberg KM, Lamprecht MR, Skouta R, Zaitsev EM, Gleason CE, Patel DN, Bauer AJ, Cantley AM, Yang WS et al. (2012) Ferroptosis: an iron-dependent form of nonapoptotic cell death. *Cell* **149**, 1060–1072.

31 Anthonymuthu TS, Tyurina YY, Sun WY, Mikulska-Ruminska K, Shrivastava IH, Tyurin VA, Cinemre FB, Dar HH, VanDemark AP, Holman TR et al. (2021) Resolving the paradox of ferroptotic cell death:

Ferrostatin-1 binds to 15LOX/PEBP1 complex, suppresses generation of peroxidized ETE-PE, and protects against ferroptosis. *Redox Biol* **38**, 101744.

32 Kagan VE, Mao G, Qu F, Angeli JP, Doll S, Croix CS, Dar HH, Liu B, Tyurin VA, Ritov VB et al. (2017) Oxidized arachidonic and adrenic PEs navigate cells to ferroptosis. *Nat Chem Biol* **13**, 81–90.

33 Hortle E, Johnson KE, Johansen MD, Nguyen T, Shavit JA, Britton WJ, Tobin DM & Oehlers SH (2019) Thrombocyte inhibition restores protective immunity to mycobacterial infection in Zebrafish. *J Infect Dis* **220**, 524–534.

34 Bafica A, Scanga CA, Serhan C, Machado F, White S, Sher A & Aliberti J (2005) Host control of Mycobacterium tuberculosis is regulated by 5-lipoxygenase-dependent lipoxin production. *J Clin Invest* **115**, 1601–1606.

35 Chen M, Divangahi M, Gan H, Shin DS, Hong S, Lee DM, Serhan CN, Behar SM & Remold HG (2008) Lipid mediators in innate immunity against tuberculosis: opposing roles of PGE2 and LXA4 in the induction of macrophage death. *J Exp Med* **205**, 2791–2801.

36 Lewis A & Elks PM (2019) Hypoxia Induces Macrophage tnfa Expression via Cyclooxygenase and Prostaglandin E2 in vivo. *Front Immunol* **10**, 2321.

37 Tobin DM, Roca FJ, Oh SF, McFarland R, Vickery TW, Ray JP, Ko DC, Zou Y, Bang ND, Chau TT et al. (2012) Host genotype-specific therapies can optimize the inflammatory response to mycobacterial infections. *Cell* **148**, 434–446.

38 Sugimoto K, Hui SP, Sheng DZ, Nakayama M & Kikuchi K (2017) Zebrafish FOXP3 is required for the maintenance of immune tolerance. *Dev Comp Immunol* **73**, 156–162.

39 Matty MA, Oehlers SH & Tobin DM (2016) Live imaging of host-pathogen interactions in Zebrafish Larvae. *Methods Mol Biol* **1451**, 207–223.

40 Wu RS, Lam II, Clay H, Duong DN, Deo RC & Coughlin SR (2018) A Rapid method for directed gene knockout for screening in G0 Zebrafish. *Dev Cell* **46**, 112–125.

41 Thisse C & Thisse B (2008) High-resolution in situ hybridization to whole-mount zebrafish embryos. *Nat Protoc* **3**, 59–69.